Supplement of Atmos. Chem. Phys., 22, 7331–7351, 2022
https://doi.org/10.5194/acp-22-7331-2022-supplement

Atmospheric Chemistry and Physics
Open Access
EGU

Supplement of

The impacts of marine-emitted halogens on OH radicals in East Asia during summer

Shidong Fan and Ying Li

Correspondence to: Ying Li (liy66@sustech.edu.cn)

Table S1. Halogen chemistry in CB6r3m mechanism. See more details in Sarwar et al. (2012) and Sarwar et al. (2019)..

Type	No.	Reaction	Rate constant / Uptake coefficient
Gaseous reactions	CL01	$Cl_2 = 2*Cl$	Photolysis
	CL02	$HOCl = OH + Cl$	Photolysis
	CL03	$Cl + O_3 = ClO + O_2$	$2.3 \times 10^{-11}\ e^{(-200/T)}$
	CL04	$ClO + ClO = 0.3*Cl_2 + 1.4*Cl + O_2$	1.63×10^{-14}
	CL05	$ClO + NO = Cl + NO_2$	$6.4 \times 10^{-12}\ e^{(290/T)}$
	CL06	$ClO + HO_2 = HOCl + O_2$	$2.2 \times 10^{-12}\ e^{(340/T)}$
	CL07	$ClO + MEO2 = Cl + FORM + HO2$	$3.2 \times 10^{-12}\ e^{(-110/T)}$
	CL08	$OH + FMCl = Cl + CO$	5.0×10^{-13}
	CL09	$FMCl = Cl + CO + HO_2$	Photolysis
	CL10	$Cl + CH_4 = HCl + MEO_2$	$6.6 \times 10^{-12}\ e^{(-1240/T)}$
	CL11	$Cl + PAR = HCl + XPAR + 0.06\ ALD2 - 0.11\ PAR + 0.76\ ROR + 0.05\ ALDX$	5.0×10^{-11}
	CL12	$Cl + PARA = HCl + ACET + 0.97\ XO_2H + 0.03\ XO_2N + RO_2 + 0.06\ ALD2 - 0.11\ PAR + 0.76\ ROR + 0.05\ ALDX$	1.4×10^{-10}
	CL13	$Cl + ETHA = HCl + 0.991\ ALD2 + 0.991\ XO_2 + 0.009\ XO_2N + HO_2$	$8.3 \times 10^{-11}\ e^{(-100/T)}$
	CL14	$Cl + ETH = FMCl + 2.0\ XO_2 + HO_2 + FORM$	1.07×10^{-10}
	CL15	$Cl + OLE = FMCl + 0.33\ ALD2 + 0.67\ ALDX + 2.0\ XO_2 + HO_2 - PAR$	2.5×10^{-10}
	CL16	$Cl + IOLE = 0.3\ HCl + 0.7\ FMCl + 0.45\ ALD2 + 0.55\ ALDX + 0.3\ OLE + 0.3\ PAR + 1.7\ XO2 + HO2 + 0.3\ OLE + 0.3\ PAR + 1.7\ XO_2 + HO_2$	3.5×10^{-10}
	CL17	$Cl + ISOP = FMCl + ISPD + 0.96\ XO_2H + 0.04\ XO_2N + RO_2$	4.3×10^{-10}
	CL18	$Cl + FORM = HCl + HO_2 + CO$	$8.2 \times 10^{-11}\ e^{(-34/T)}$
	CL19	$Cl + ALD2 = HCl + C_2O_3$	7.9×10^{-11}
	CL20	$Cl + ALDX = HCl + C_XO_3$	1.3×10^{-10}
	CL21	$Cl + MEOH = HCl + HO_2 + FORM$	5.5×10^{-11}
	CL22	$Cl + ETOH = HCl + HO_2 + ALD2$	$8.2 \times 10^{-11}\ e^{(45/T)}$
	CL23	$OH + HCl = Cl + H_2O$	$6.58 \times 10^{-13}\ (T/300)^{1.16}\ e^{(58/T)}$
	CL24	$Cl + TOL = HCl + 0.18*CRES + 0.65*TO_2 + 0.72*RO_2 + 0.1*OPEN + 0.1*OH + 0.07*XO_2H + 0.18*HO_2 + TOLRO_2$	6.1×10^{-11}
	CL25	$Cl + XYLMN = HCl + 0.155*CRES + 0.544*XLO_2 + 0.602*RO_2 + 0.244*XOPN + 0.244*OH + 0.058*XO_2H + 0.155*HO_2 + XYLRO_2$	1.2×10^{-10}
	CL26	$Cl + NAPH = HCl + 0.155*CRES + 0.544*XLO_2 + 0.602*RO_2 + 0.244*XOPN + 0.244*OH + 0.058*XO_2H + 0.155*HO_2 + XYLRO_2$	1.2×10^{-10}
	CL27	$ClNO_2 = Cl + NO_2$	Photolysis
	CL28	$ClO + NO_2 = ClNO_3$	$k_o = 1.8 \times 10^{-31}\ (T/300)^{-3.4}$; $k_\infty = 1.5 \times 10^{-11}\ (T/300)^{-1.9}$; $F = 0.6$ and $N = 1.0$
	CL29	$ClNO_3 = ClO + NO_2$	Photolysis
	CL30	$ClNO_3 = Cl + NO_3$	Photolysis
	BR01	$Br + O_3 = BrO + O_2$	$1.6\times 10^{-11}e^{-780/T}$
	BR02	$BrO + HO_2 = HOBr + O_2$	$4.5\times 10^{-12}e^{460/T}$
	BR03	$Br + HO_2 = HBr + O_2$	$4.8\times 10^{-12}\ e^{-310/T}$
	BR04	$HBr + OH = Br + H_2O$	$6.7\times 10^{-12}e^{155/T}$
	BR05	$BrO + BrO = 2.0\ Br + O_2$	$1.4\times 10^{-12}e^{210/T}$
	BR06	$BrO + BrO = BR_2 + O_2$	$2.9 \times 10^{-14}e^{840/T}$
	BR07	$BrO + NO = Br + NO_2$	$8.8\times 10^{-12}e^{260/T}$
	BR08	$Br + BrNO_3 = BR_2 + NO_3$	4.9×10^{-11}
	BR09	$BR_2 + OH = HOBr + Br$	$2.1\times 10^{-11}e^{240/T}$
	BR10	$BrO + OH = Br + HO_2$	$1.7\times 10^{-11}e^{250/T}$
	BR11	$Br + NO_3 = BrO + NO_2$	1.6×10^{-11}
	BR12	$BrO + NO_2 = BrNO_3$	$k_o = 5.2 \times 10^{-31}(T/300)^{-3.2}$; $k_\infty = 6.9 \times 10^{-12}(T/300)^{-2.9}$; $F = 0.6$ and $N = 1.0$
	BR13	$Br + NO_2 = BrNO_2$	$k_o = 4.2 \times 10^{-31}(T/300)^{-2.4}$; $k_\infty = 2.7 \times 10^{-11}(T/300)^{0.0}$; $F = 0.6$ and $N = 1.0$
	BR14	$BrO + ClO = Br + Cl$	$4.7 \times 10^{-12}e^{320/T}$
	BR15	$Br + FORM = HBr + HO_2 + CO$	$1.7 \times 10^{-11}e^{-800/T}$
	BR16	$Br + ALD2 = HBr + C_2O_3$	$1.3 \times 10^{-11}e^{-360/T}$

Table S1. Continued.

Type	No.	Reaction	Rate constant / Uptake coefficient
	BR17	$Br + OLE = FMBr + ALD2 + XO_2H - PAR + RO_2$	3.6×10^{-12}
	BR18	$Br + ISOP = FMBr + ISPD + 0.96\ XO_2H + 0.04\ XO_2N + RO_2$	5.0×10^{-12}
	BR19	$FMBr + OH = BR + CO$	5.0×10^{-12}
	BR20	$BrO + MEO2 = 0.8\ HOBr + 0.2\ BR + FORM$	$2.7 \times 10^{-14} e^{1600/T}$
	BR21	$CH_3Br + OH = Br + FORM$	$2.9\times 10^{-12}e^{-1230/T}$
	BR22	$MB3 + OH = 3\ Br + CO$	$1.0\times 10^{-12}e^{-388/T}$
	BR23	$MB2 + OH = 2\ Br + HO2 + CO$	$2.0\times 10^{-12}e^{-840/T}$
	BR24	$MB2C + OH = 2\ Br + Cl + CO$	$9.0\times 10^{-13}e^{-420/T}$
	BR25	$MBC2 + OH = Br + 2\ Cl + CO$	$9.4 \times 10^{-13}e^{-510/T}$
	BR26	$MBC + OH = Br + Cl + CO + HO2$	$2.1\times 10^{-12}e^{-880/T}$
	BR27	$DMS + BrO = MEO2 + Br$	$1.5 \times 10^{-14}e^{1000/T}$
	BR28	$Br_2 = 2\ Br$	Photolysis
	BR29	$HOBr = OH + Br$	Photolysis
	BR30	$BrO = Br + O$	Photolysis
	BR31	$BrNO_2 = Br + NO_2$	Photolysis
	BR32	$BrNO_3 = BrO + NO_2$	Photolysis
	BR33	$BrNO_3 = Br + NO_3$	Photolysis
	BR34	$BrCl = Br + Cl$	Photolysis
	BR35	$FMBr = Br + CO + HO_2$	Photolysis
	BR36	$MB3 = 3\ Br + HO2 + CO$	Photolysis
	BR37	$MB2C = 2\ Br + Cl + HO2 + CO$	Photolysis
	BR38	$MBC2 = Br + 2\ Cl + HO2 + CO$	Photolysis
	IO01	$I + O_3 = IO + O_2$	$2.1 \times 10^{-11}e^{-830/T}$
	IO02	$I + HO_2 = HI + O_2$	$1.5 \times 10^{-11}e^{-1090/T}$
	IO03	$I_2 + OH = HOI + I$	2.1×10^{-10}
	IO04	$HI + OH = I + H_2O$	$1.6 \times 10^{-11}e^{440/T}$
	IO05	$HOI + OH = IO + H_2O$	5.0×10^{-12}
	IO06	$IO + HO_2 = HOI + O_2$	$1.4 \times 10^{-11}e^{540/T}$
Gaseous reactions	IO07	$IO + NO = I + NO_2$	$7.15 \times 10^{-12}e^{300/T}$
	IO08	$INO + INO = I_2 + 2\ NO$	$8.4 \times 10^{-11}e^{-2620/T}$
	IO09	$INO_2 + INO_2 = I2 + 2\ NO_2$	$4.7 \times 10^{-13}e^{-1670/T}$
	IO10	$I_2 + NO_3 = I + INO_3$	1.5×10^{-12}
	IO11	$INO_3 + I = I_2 + NO_3$	$9.1 \times 10^{-11}e^{-146/T}$
	IO12	$I + BrO = IO + Br$	1.2×10^{-11}
	IO13	$IO + Br = I + BrO$	2.70×10^{-11}
	IO14	$IO + BrO = Br + I + O_2$	$1.5\times 10^{-11}e^{510/T}$
	IO15	$IO + ClO = I + Cl$	$4.7\times 10^{-12}e^{280/T}$
	IO16	$OIO + OIO = I_2O_4$	$1.5 \times 10^{-10}e^{0/T}$
	IO17	$OIO + NO = IO + NO_2$	$1.1 \times 10^{-12}e^{542/T}$
	IO18	$IO + IO = 0.4OIO + 0.4I + 0.6I_2O_2$	$5.4 \times 10^{-11}e^{180/T}$
	IO19	$IO + OIO = I_2O_3$	1.5×10^{-10}
	IO20	$I_2O_2 = OIO + I$	$2.5 \times 10^{14} e^{-9770/T}$
	IO21	$I_2O_4 = 2OIO$	$3.8 \times 10^{-2}e^{0/T}$
	IO22	$INO_2 = I + NO_2$	$9.94 \times 10^{17} e^{-11859/T}$
	IO23	$INO_3 = IO + NO_2$	$2.1 \times 10^{15} e^{-13670/T}$
	IO24	$I + NO = INO$	$k_o = 1.8 \times 10^{-32}(T/300)^{-1.0}$; $k_\infty = 1.7 \times 10^{-11}(T/300)^{-0.0}$; F = 0.6 and N = 1.0
	IO25	$I + NO_2 = INO_2$	$k_o = 3.0 \times 10^{-31}(T/300)^{-1.0}$; $k_\infty = 6.6 \times 10^{-11}(T/300)^{-0.0}$; F = 0.6 and N = 1.0
	IO26	$IO + NO_2 = INO_3$	$k_o = 7.7 \times 10^{-31}(T/300)^{-5.0}$; $k_\infty = 1.6 \times 10^{-11}(T/300)^{-0.4}$; F = 0.4 and N = 1.0
	IO27	$CH_3I + OH = I + HO_2 + H_2O$	$4.3\times 10^{-12}e^{-1120//T}$
	IO28	$IO + DMS = I + MEO2$	$3.2 \times 10^{-13}e^{-925/T}$
	IO29	$CH_3I = I + MEO2$	Photolysis

Table S1. Continued.

Type	No.	Reaction	Rate constant / Uptake coefficient
Gaseous reactions	IO30	CH_2I_2= 2.0 I	Photolysis
	IO31	CH_2IBr = I + Br	Photolysis
	IO32	CH_2ICl = I + Cl	Photolysis
	IO33	I_2= 2.0 I	Photolysis
	IO34	IO = I + O	Photolysis
	IO35	OIO = I + O_2	Photolysis
	IO36	INO = I + NO	Photolysis
	IO37	INO_2 = I + NO_2	Photolysis
	IO38	INO_3= I + NO_3	Photolysis
	IO39	HOI = I + OH	Photolysis
	IO40	ICl = I + Cl	Photolysis
	IO41	I_2O_2= I + OIO	Photolysis
	IO42	I_2O_3= IO + OIO	Photolysis
	IO43	I_2O_4= OIO + OIO	Photolysis
	IO44	IBr = I + Br	Photolysis
Heterogeneous reactions on aerosols	HET_CLNO3_WA	$ClNO_3$ → HOCl + HNO_3	0.024
	HET_N2O5	Cl- + N_2O_5 → $ClNO_2$	Parameterization from
	HET_HBR_BR	HBr →Br^-	$1.3\times 10^{-8}e^{4290/T}$
	HET_BRNO3_WA	$BrNO_3$(+ H_2O)→HOBr + HNO_3	0.03
	HET_HOBR_CL	HOBr + Cl^-→BrCl	0.08
	HET_HOBR_BR	HOBr + Br^-→Br_2	0.02
	HET_I2O2	I_2O_2→	0.02
	HET_I2O3	I_2O_3→	0.02
	HET_I2O4	I_2O_4 →	0.02
	HET_INO3_CL	INO_3 + Cl^-→ICl + HNO_3	0.005
	HET_INO3_BR	INO_3 + Br^-→IBr + HNO_3	0.005
	HET_INO2_CL	INO_2 + Cl^-→ICl + HONO	0.01
	HET_INO2_BR	INO_2 + Br^-→IBr + HONO	0.01
	HET_HOI_CL	HOI + Cl^-→ICl	0.005
	HET_HOI_BR	HOI + Br^-→IBr	0.005
Heterogeneous reactions on ice crystals	HET_HOBR_HBR	HOBr + HBr →Br_2 + H_2O	0.12
	HET_HOBR_HCL	HOBr + HCl →BrCl + H_2O	0.30
	HET_HOCL_HBR	HOCl + HBr →BrCl + H_2O	0.20

Note. First order rate constants are in units of s^{-1}, second order rate constants are in units of cm^3 $molecule^{-1}$ s^{-1}. Temperatures (T) are in Kelvin. k_o, k_∞, F, and N are for rate constants described by the falloff expression of the form $k = \{k_o[M]/(1 + k_o[M]/k_\infty)\}$ F^Z, where $Z = \{(1/N) + \log_{10}[k_o [M]/ k_\infty]^2\}^{-1}$, where [M] is the total pressure in molecules cm^{-3}.

ACET = acetone, ALD2 = acetaldehyde, ALDX = propionaldehyde and higher aldehydes, C2O3 = acetylperoxy radical, CRES = cresol and higher molecular weight phenols, CXO3 = higher acylperoxy radicals, ETH = ethene, ETHA = ethane, ETOH=ethanol, FMBr = formyl bromide, FMCl = formyl chloride, FORM = formaldehyde, IOLE = internal olefinic carbon bond, ISOP = isoprene, ISPD = isoprene product, MEO2 = methylperoxy radical, MEOH = methanol, NAPH = naphthalene, OLE = terminal olefinic carbon bond, RO_2 = peroxy radical ROR = secondary alkoxy radical, PAR = paraffin carbon bond, TOL = toluene, XLO_2 = peroxy radical from XYLMN+OH reaction, XO_2 = NO-to-NO_2 operator, XO_2N = NO-to-nitrate operator, XO_2H = NO-to-NO_2 with HO_2 production, from alkoxy radicals, XOPN = product of aromatic ring-opening reaction, XPAR = organic nitrate production from PAR, XYLMN = xylene and other polyalkyl aromatics except naphthalene, $XYLRO_2$ = counter species for aerosol from XYLMN+OH.

Table S2. Global annual fluxes of very short-lived halocarbons reported in previous studies and scale factors of halocarbon emissions used in this study.

Species	Annual flux **(Gg/yr)**			Scale factor	
	Ordóñez et al. (2012)	**WMO low**	**WMO high**	**low**	**high**
$CHBr_3$	533	126	865	0.24	1.62
CH_2Br_2	67.3	62	109	0.92	1.62
CH_3I	303	176	615	0.58	2.03
CH_2BrCl	10.0	6.48	9.72	0.65	1
$CHBr_2Cl$	19.7	19.6	56.1	1	2.85
$CHBrCl_2$	22.6	16.4	22.6	0.73	1
CH_2ICl	234	--	--	0.58	2.03
CH_2IBr	87.3	--	--	0.58	2.03
CH_2I_2	116	--	--	0.58	2.03

Table S3. Case design in the supplementary information.

Simulation case	Species or reactions[a]	Emission rate and ref
BASE_PHIL5	As BASE but increasing NOx and VOCs emissions in the Philippines by a factor of 5, corresponding to InorgI_chemPHIL5 below.	0
All_highI	As All_high	Replacing HOI emission with I_2 in equivalent amount of I atom
InorgI_chemIhalf	As InorgI_chem	Decreasing I_2 and HOI emission rates by 50%
InorgI_chemIfixed	As InorgI_chem	Fixing I_2 and HOI emission rates over the domain and time
InorgI_chemPHIL5	As InorgI_chem but increasing NOx and VOCs emissions in the Philippines by a factor of 5.	As in InorgI_chem

35

Table S4. Cross reference between cases and figures.

Figures	Cases
Fig. 1	All_high
Fig. 2	All_high − BASE All_low − BASE
Fig. 3	All_high − BASE
Fig. 4	(a)–(d) SSA: SSA − BASE (e)–(h) InorgI: InorgI − BASE (i)–(l) HaloC: HaloC − BASE (m)–(p) interaction: All_high – SSA – InorgI – HaloC + 2BASE
Fig. 5, decomposition of Figs. 4a–d	(a)–(d) SSA_phy: SSA_phy − BASE_phy (e)–(h) SSA_chemCl: (SSA_Cl − BASE) − (SSA_phy − BASE_phy) (i)–(l) SSA_chemBr: SSA − SSA_Cl
Fig. 6	Corresponding to values in Figs. 5 and 7 divided by BASE
Fig. 7, decomposition of Figs. 4e–h	(a)–(d) O_3depo: InorgI − InorgI_chem (e)–(h) InorgI_chem: InorgI_chem − BASE
Fig. 8	All_high
Fig. 9	InorgI_chem
Fig. S1	All_high, All_low, BASE
Fig. S2	All_high, BASE
Fig. S3	All_low − BASE
Fig. S4	(a) All_high – BASE (b) SSA – SSA_Cl
Fig. S5	--
Fig. S6	SSA_phy
Fig. S7	SSA_Cl, BASE
Fig. S8	(a)–(b) All_high − BASE (c) All_high – All_highI (d) (InorgI_chem – BASE) + (All_highI – All_high)
Fig. S9	(a) InorgI_chemIhalf − BASE (b)–(c) InorgI_chemIhalf − InorgI_chem (d) InorgI_chemIfixed − BASE (e)–(f) InorgI_chemIfixed − InorgI_chem
Fig. S10	(a) BASE_PHIL5 − BASE (b) InorgI_chemPHIL5 – BASE_PHIL5 (c)–(f) (InorgI_chemPHIL5 – BASE_PHIL5) − (InorgI_chem − BASE)

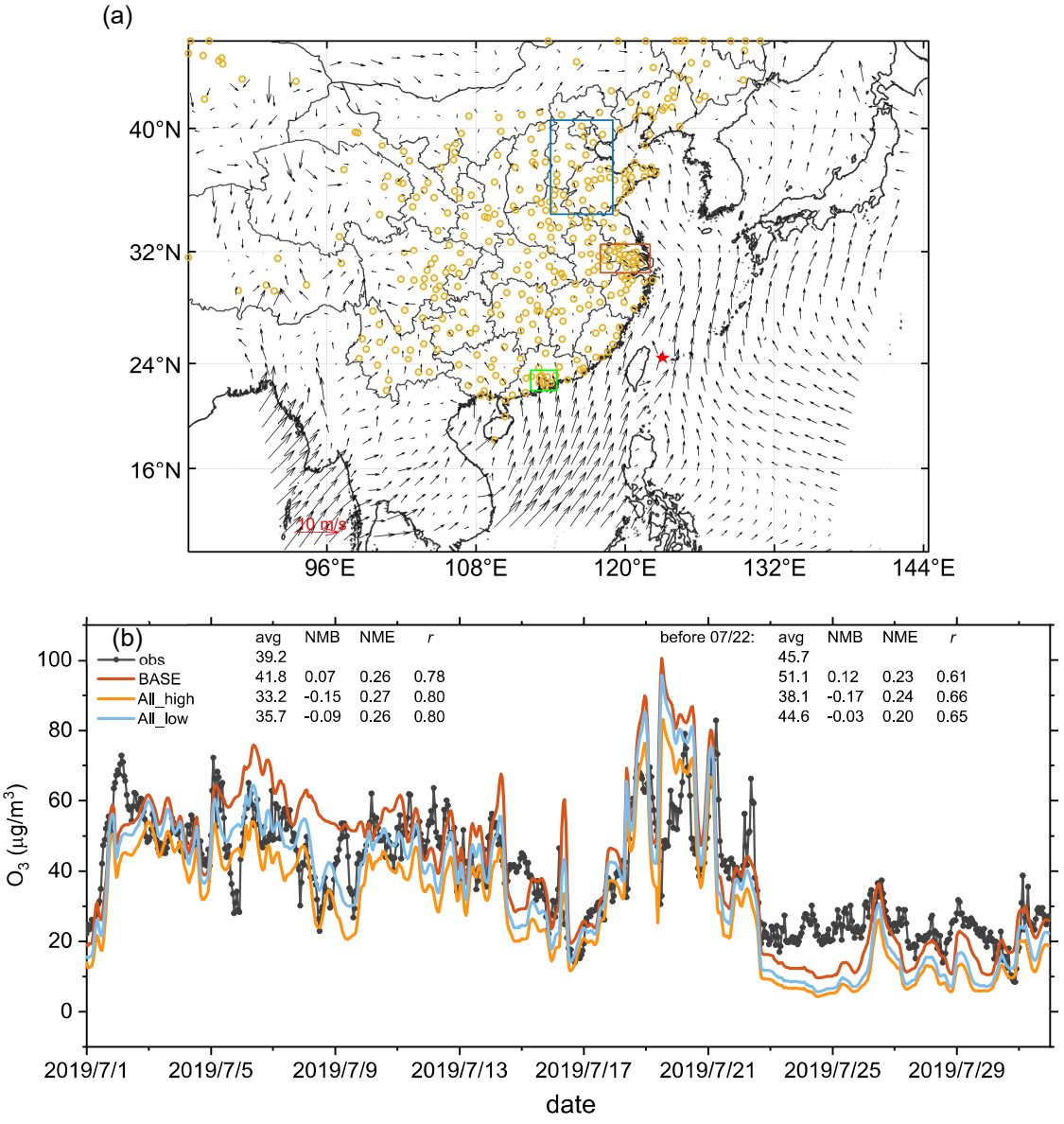

Figure S1. (a) Positions of the observation stations for model evaluation. The yellow circles are stations. The blue, orange, and green boxes indicate the North China Plain, the Yangtze River Delta, and the Pearl River Delta areas, respectively. The red star East to the Taiwan island is the location of the Yonaguni station. The arrows indicate the monthly averaged wind field. (b) Simulated and measured O_3 concentration at Yonaguni. The variation of O_3 in July 2019 here is reasonably captured by all the three simulations. Adding the halogen emissions (especially with low emission rates) can noticeably lower the bias for the high ozone concentration and improve the correlation between observation and simulations -relationship (i.e., days before July 22).

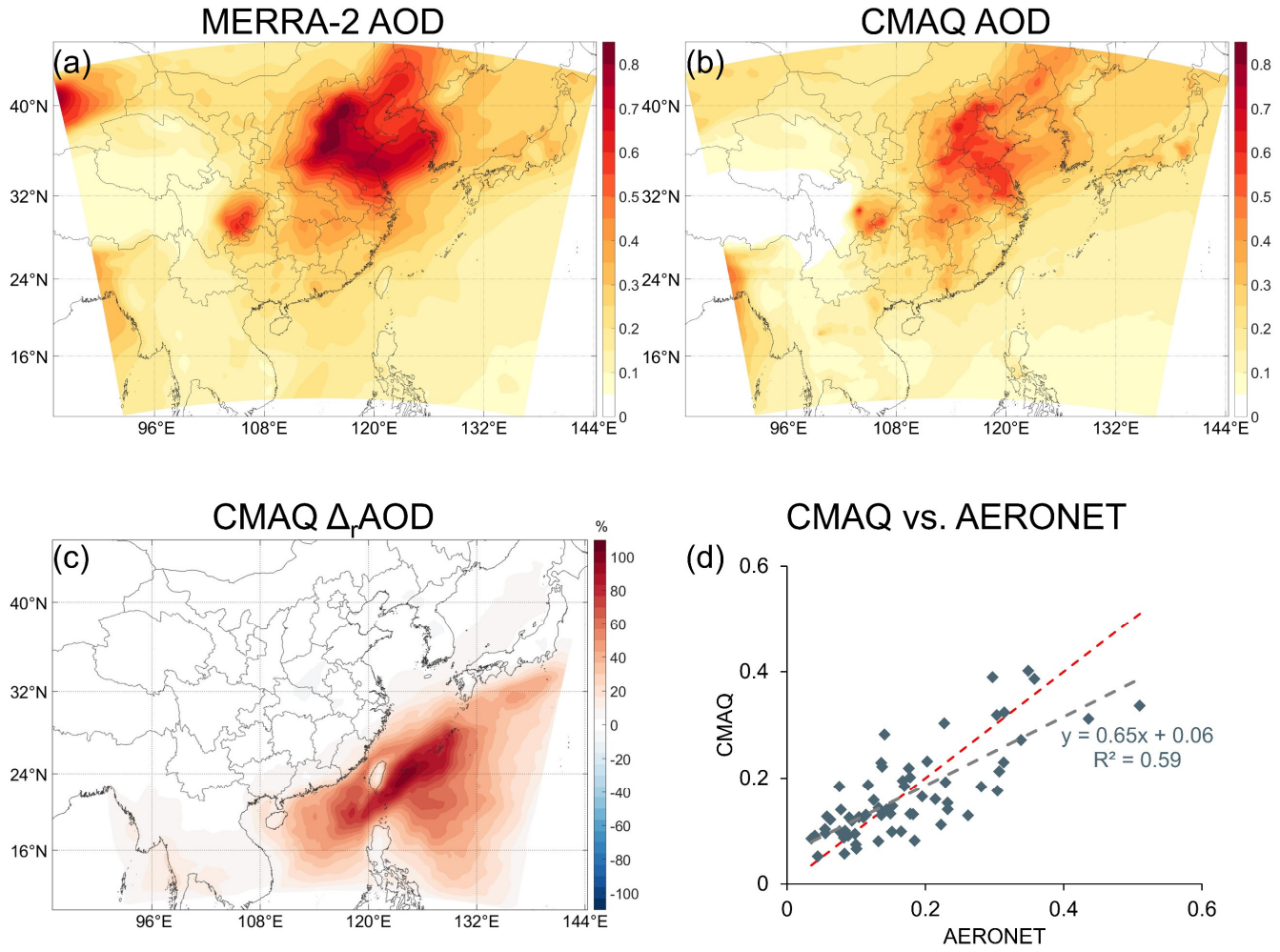

Figure S2. Spatial distribution of (a) MERRA-2 (downloaded from https://disc.gsfc.nasa.gov/datasets/M2TMNXAER_5 .12 .4/summary?keywords=MERRA-2%20AOD) and (b) modelled (in All_high case) monthly average of AOD, and (c) relative change of AOD due to the emission of SSA ((3high−BASE)/BASE). (d) The comparison of daily modelled AOD in All_high case and AERONET AOD (550nm calculated from 500nm using Angstrom exponent) at four available island stations (north to south: Fukue, Okinawa_Hedo, Dongsha, and Manila, https://aeronet.gsfc.nasa.gov/cgi-bin/webtool_aod_v3?stage=2&region=Asia). All AOD data are at 550 nm.

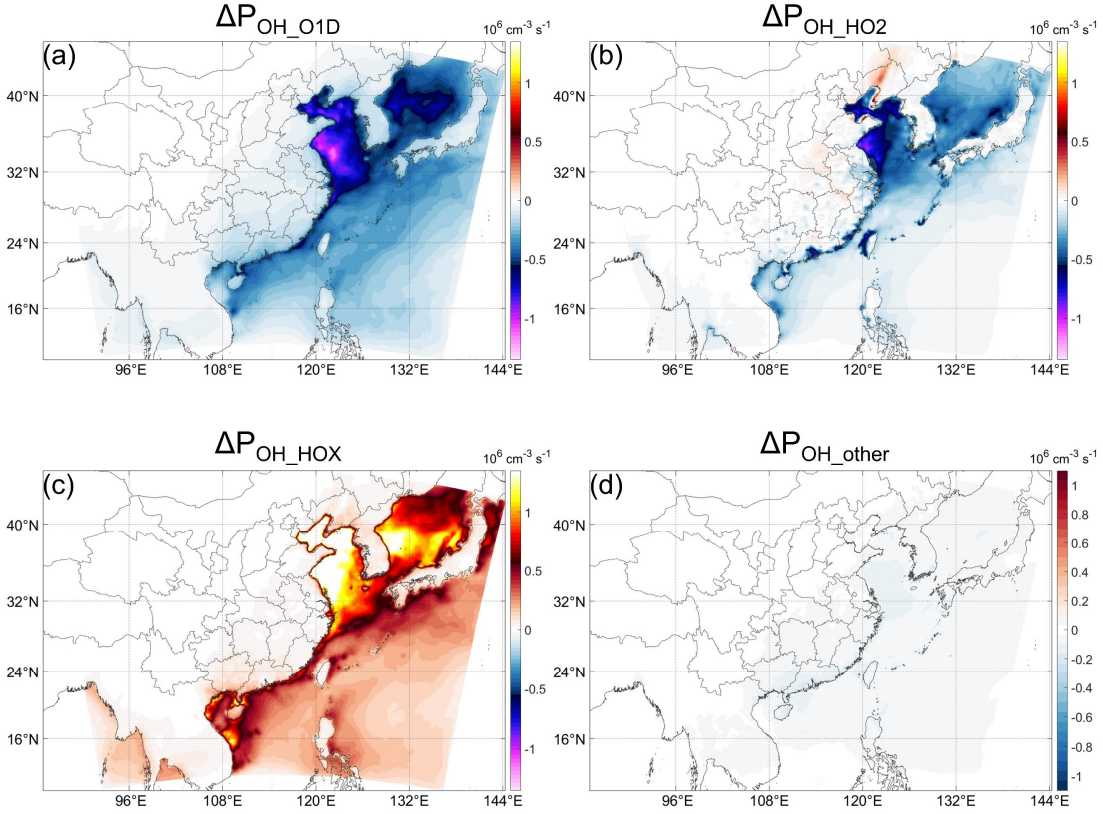

Figure S3. The same as Fig. 3 but for All_low case. The red and blue color scales are the same in (a)–(d).

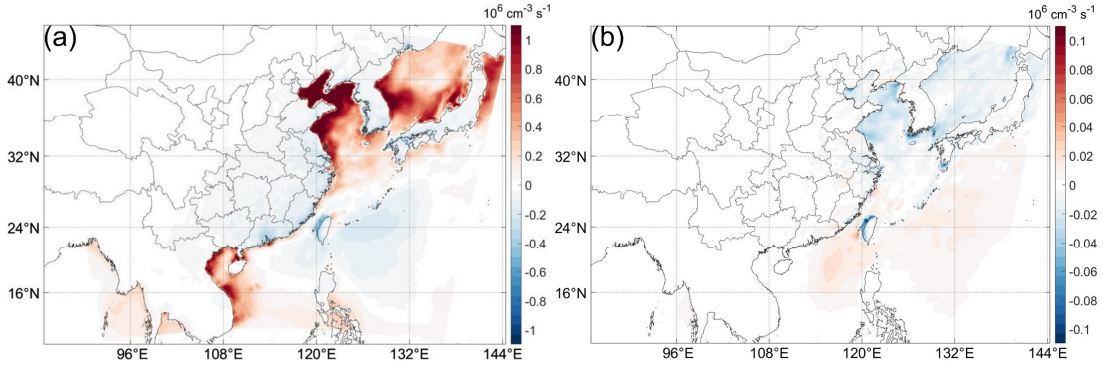

Figure S4. Change of P_{OH} (a) through pathway 1 (ΔP_{OH_O1D}) and 3 (ΔP_{OH_HOX}) in All_high case compared to BASE case, and (b) through pathway 2 (ΔP_{OH_HO2}) and 3 (ΔP_{OH_HOX}) in "SSA_chemBr" case compared to BASE case.

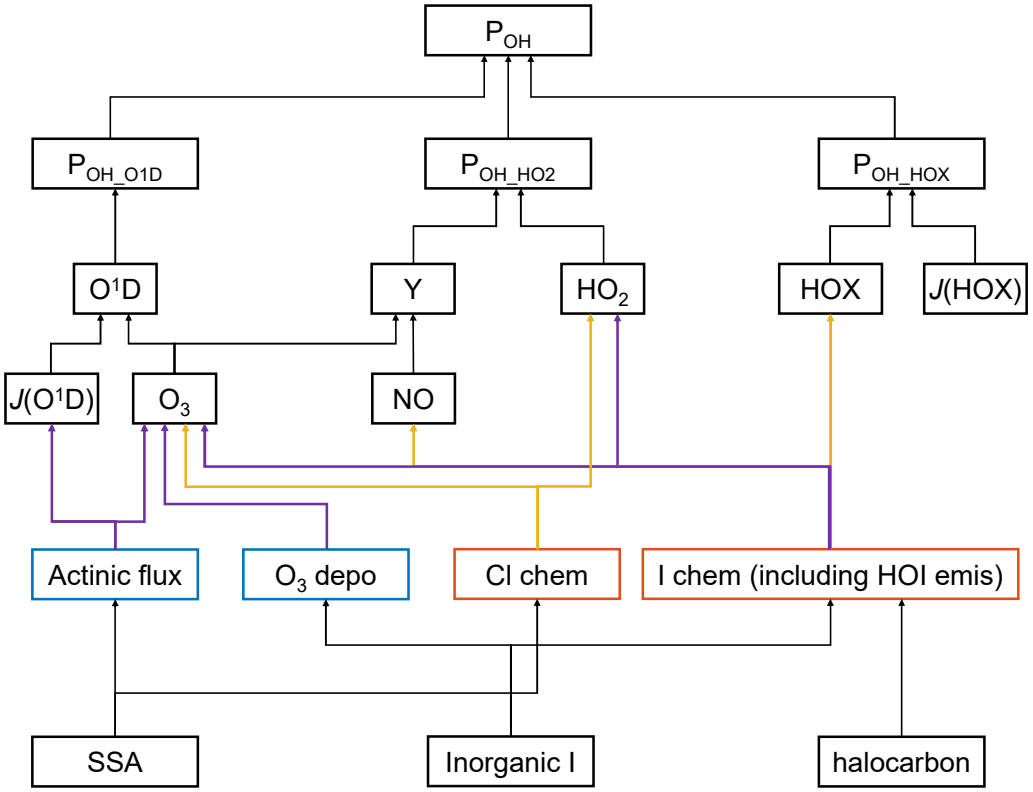

Figure S5. Schematic representation of the three main pathways that halogen species influence OH production (P_{OH_O1D}, P_{OH_HO2}, and P_{OH_HOX}) and their main controlling factors. The boxes in blue and orange represent independent and interrelated (chemical) factors, respectively. The purple and yellow arrows represent decrease and increase of the target species or parameters, respectively.

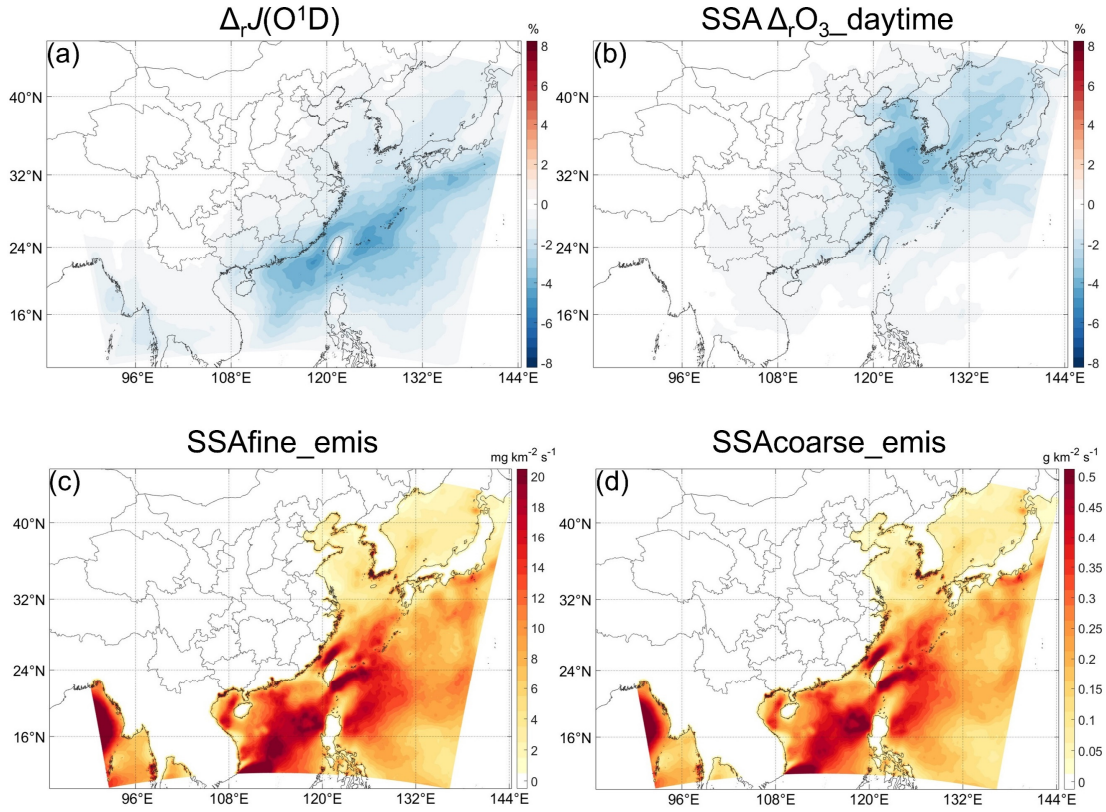

Figure S6. Relative change of (a) $J(O^1D)$ and (b) daytime O_3 caused by the extinction effect of SSA, approximated by Δ_rO_3_daytime in SSA_Cl without the uptake of N_2O_5 and yield of $ClNO_2$. (c) Monthly averaged emission rate of fine (≤2.5 μm) SSA. (d) Monthly averaged emission rate of coarse (>2.5 μm) SSA.

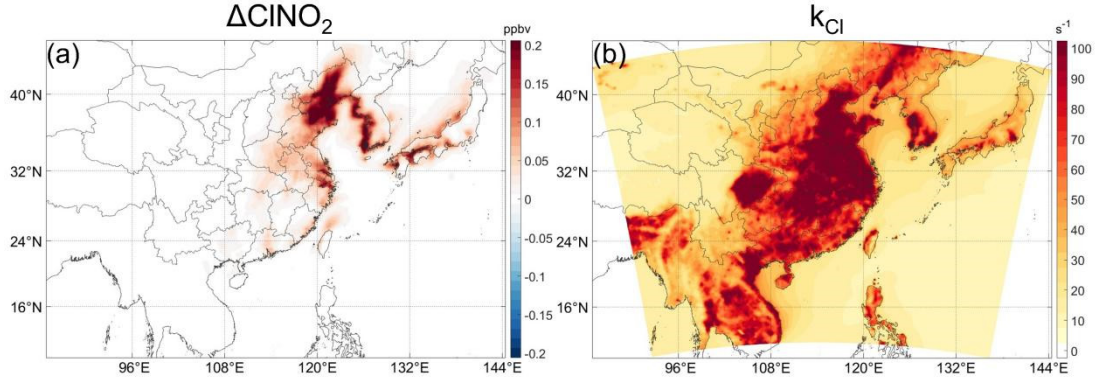

Figure S7. (a) $ClNO_2$ change in SSA_Cl case compared to BASE case. (b) k_{Cl} in BASE case (Δk_{Cl} is very small).

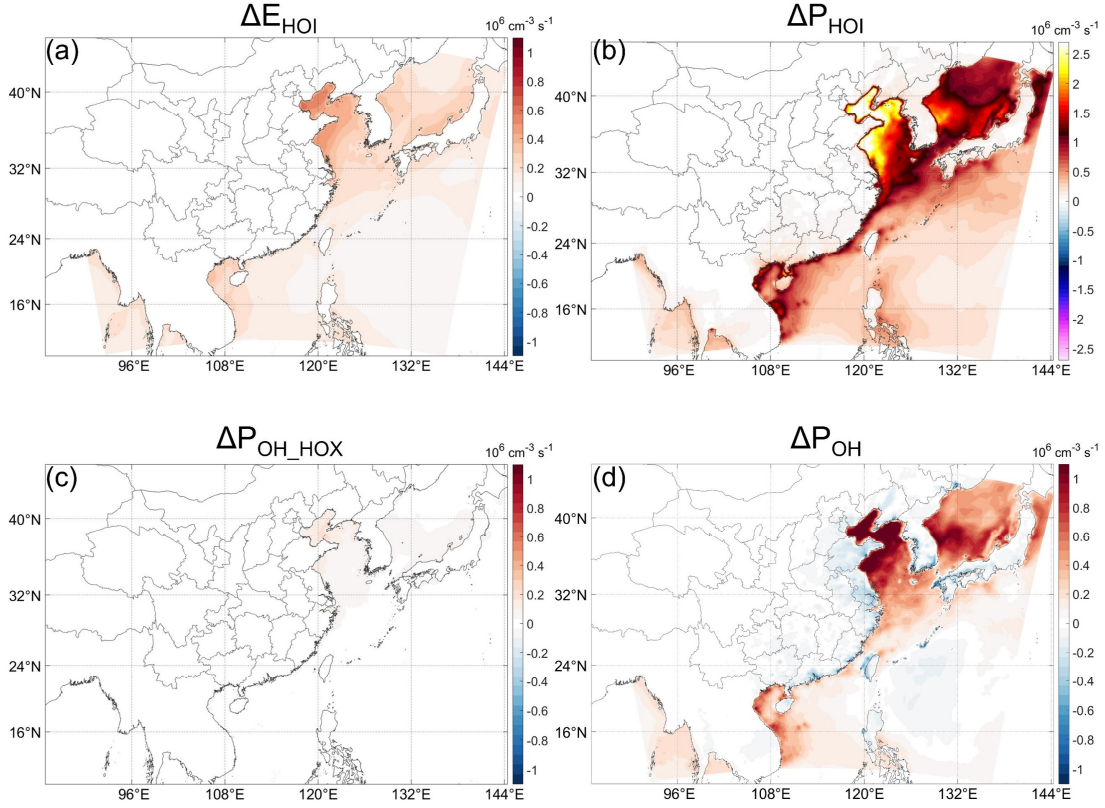

Figure S8. Change of HOI (a) emission rate and (b) production rate from HO_2+IO in All_high case compared to BASE case. (c) Change of P_{OH_HOX} by replacing HOI emission with an equivalent amount of I_2 in All_high case, approximating the contribution of direct HOI emission to P_{OH_HOX}. The very small values in (c) indicates that what is more important in the iodine chemistry is the amount of reactive inorganic iodine, no matter what the form is (HOI or I_2). (d) ΔP_{OH} induced by iodine chemistry with HOI emission replaced by I_2 in InorgI_chem case (compare with Fig. 7e), approximated using All_high data.

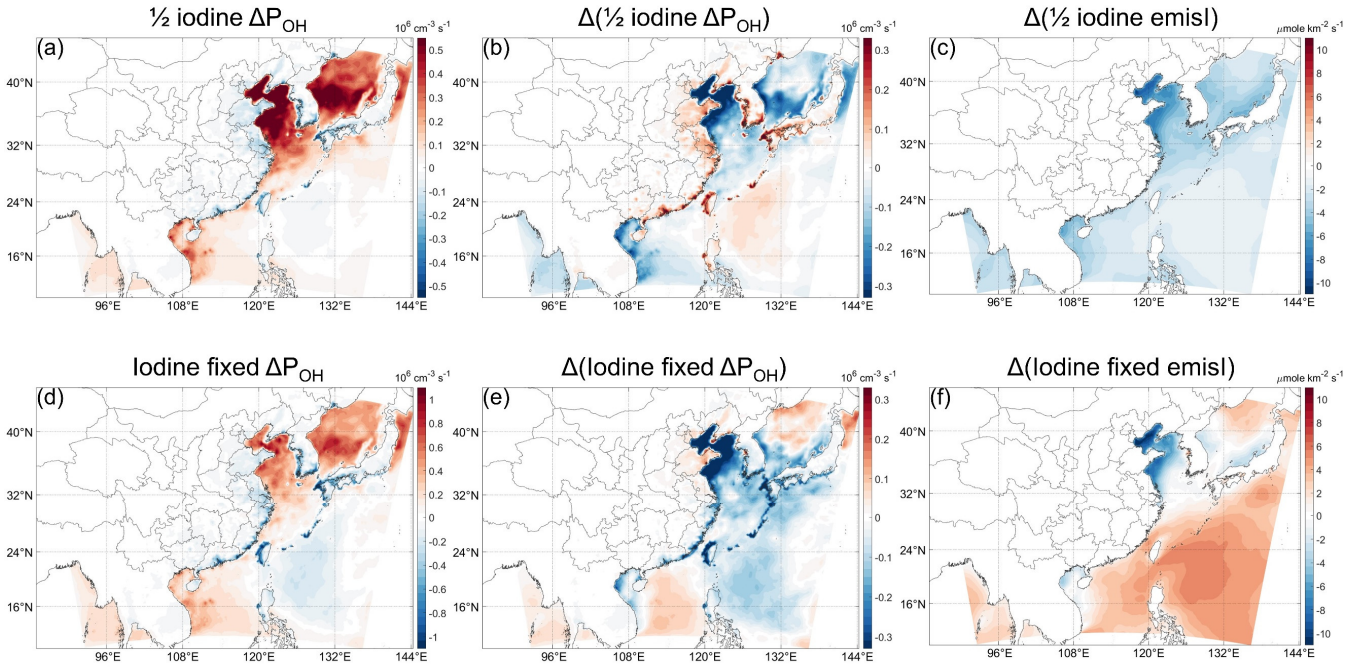

Figure S9. P_{OH} change and emission rate in a case reducing inorganic iodine emissions by 50% relative to InorgI_chem case (a–c) and in a case with fixed emission rate of iodine (6.86=5000/27^2 μmole km^{-2} s^{-1} for HOI, and 1/20 of HOI for I_2) (d–f). (a) The same as Fig. 4e but with reduced the HOI/I_2 emission rates. (b) The difference between (a) and Fig. 4e. (c) The reduction of emission rate of iodine (HOI+2×I_2). Note the different scales. (d)–(f) are the same as (a)–(c) but with fixed emission rate of iodine.

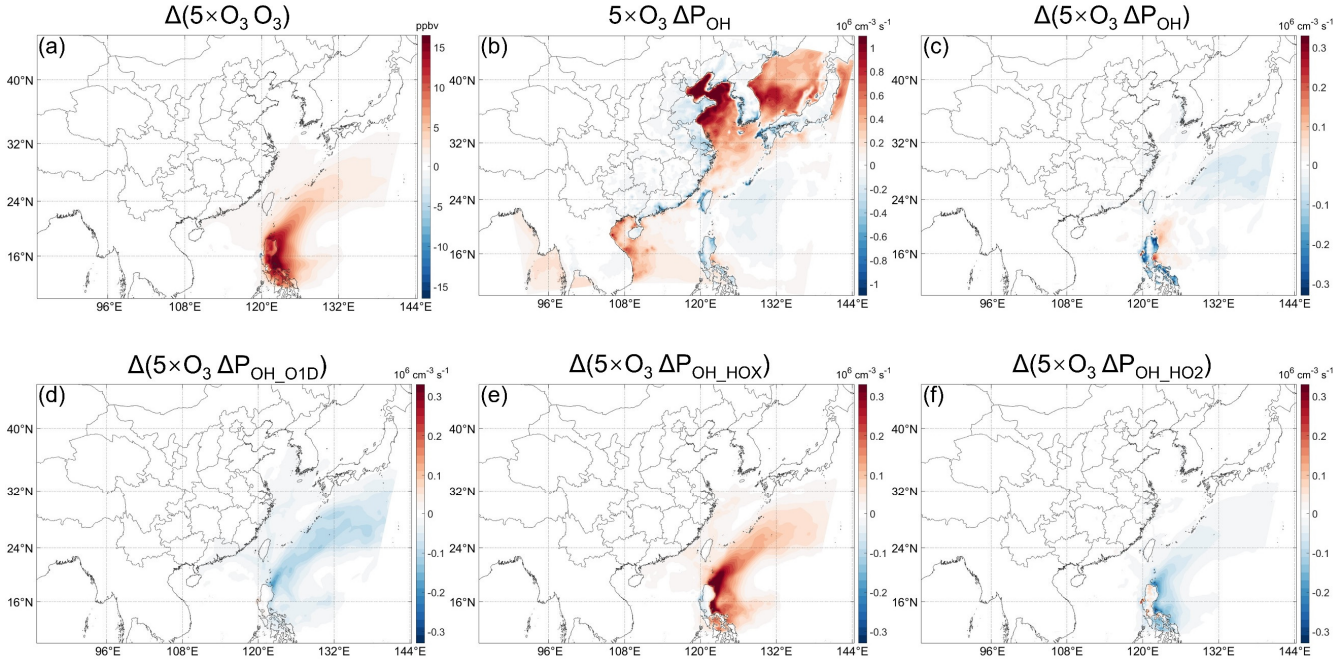

Figure S10. (a) O_3 increase in BASE case when increasing NO*x* and VOCs emissions by a factor of five in the Philippines, "Δ" before the parenthesis indicated BASE with increased O_3 minus BASE. (b) P_{OH} change induced by iodine chemistry in the case with increased NO*x* and VOCs emissions (both BASE and InorgI_chem cases increase the emissions), the same as Fig. 4e except the NO*x* and VOCs emissions. (c) The difference between (a) and Fig. 4e, characterizing the further change of P_{OH} induced by iodine chemistry when increasing O_3 concentration. (d)–(f) The three main pathways decomposing (c). Note the different scales. (c) illustrates a striking characteristic of the further ΔP_{OH} over the ocean: positive close to the source, negative far away; in the continent, the negative further ΔP_{OH} is caused by the other pathways than the main three (d)–(f), which is not discussed further here.

References

Ordóñez, C., Lamarque, J. F., Tilmes, S., Kinnison, D. E., Atlas, E. L., Blake, D. R., Santos, G. S., Brasseur, G., and Saiz-Lopez, A.: Bromine and iodine chemistry in a global chemistry-climate model: description and evaluation of very short-lived oceanic sources, Atmospheric Chemistry and Physics, 12, 1423-1447, 10.5194/acp-12-1423-2012, 2012.

Sarwar, G., Simon, H., Bhave, P., and Yarwood, G.: Examining the impact of heterogeneous nitryl chloride production on air quality across the United States, Atmospheric Chemistry and Physics, 12, 6455-6473, 10.5194/acp-12-6455-2012, 2012.

Sarwar, G., Gantt, B., Foley, K., Fahey, K., Spero, T. L., Kang, D. W., Mathur, R., Foroutan, H., Xing, J., Sherwen, T., and Saiz-Lopez, A.: Influence of bromine and iodine chemistry on annual, seasonal, diurnal, and background ozone: CMAQ simulations over the Northern Hemisphere, Atmospheric Environment, 213, 395-404, 10.1016/j.atmosenv.2019.06.020, 2019.